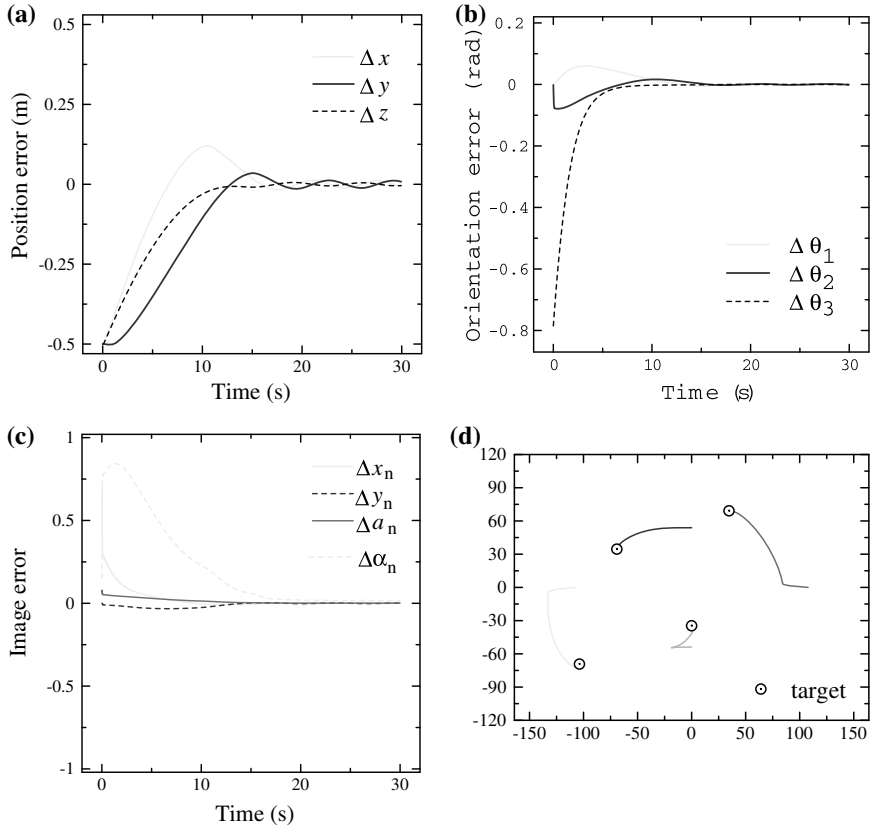

Figure 11. Simulation results in Case 5, con gured as Figure 7

Downloaded by [Inria Rocquencourt] at 08:14 05 April 2013

plane parallel to the image plane. The robustness of these approximations will be con rmed in the simulations.

5. Stability analysis

In this section, we prove the stability of the system (12) at the equilibrium point $(\boldsymbol{p}, \boldsymbol{z}) = (\boldsymbol{p}^*, \mathbf{0})$ using the controller (56). Using Equations (14) and (56), the closed loop of the system becomes

$$\begin{aligned} m\ddot{\boldsymbol{x}} &= -\boldsymbol{b}_1 + {}^{w}\boldsymbol{R}_r\{\boldsymbol{h}_g - \boldsymbol{P}_{s_{v_1}}^{\top}\boldsymbol{K}_v\Delta\boldsymbol{s}_v\}\boldsymbol{H}\ddot{\boldsymbol{\theta}} + \frac{1}{2}\boldsymbol{H}\boldsymbol{\theta} \\ &= -\boldsymbol{S}\boldsymbol{\theta} - \boldsymbol{b}_2 - \boldsymbol{G}^{\top}\left\{\boldsymbol{H}_h^{\top}\Delta\boldsymbol{s}_h + \boldsymbol{P}_{s_{v_2}}^{\top}\boldsymbol{K}_v\Delta\boldsymbol{s}_v \right. \\ &\quad \left. + [{}^{r}\boldsymbol{y}_{sen}]_{\times}\boldsymbol{K}\Delta\,{}^{r}\boldsymbol{y}_{sen} + \gamma\,{}^{r}\boldsymbol{\omega}\right\}. \end{aligned} \tag{57}$$

To prove the stability of the system, we choose the following as the candidate of the Lyapunov function,

$$V = \frac{1}{2}\left\{m\,\|\dot{\boldsymbol{x}}\|^2 + \boldsymbol{\theta}^{\top}\boldsymbol{H}\boldsymbol{\theta}\right\} + \sum_{i=1}^{3} V_i, \tag{58}$$

where V_i ($i = 1, 2, 3$) is de ned in Eqs. (35), (39) and (53). This function is obviously positive de nite. Then, the time derivative of V is given as follows:

$$\begin{aligned} \dot{V} &= m\dot{\boldsymbol{x}}^{\top}\ddot{\boldsymbol{x}} + \boldsymbol{\theta}^{\top}\left(\boldsymbol{H}\ddot{\boldsymbol{\theta}} + \frac{1}{2}\dot{\boldsymbol{H}}\boldsymbol{\theta}\right) + {}^{r}\boldsymbol{v}^{\top}\boldsymbol{P}_{s_{v1}}^{\top}\boldsymbol{K}_v\Delta\boldsymbol{s}_v \\ &\quad + {}^{r}\boldsymbol{\omega}^{\top}\boldsymbol{P}_{s_{v2}}^{\top}\boldsymbol{K}_v\Delta\boldsymbol{s}_v + {}^{r}\boldsymbol{\omega}^{\top}\boldsymbol{H}_h^{\top}\Delta\boldsymbol{s}_h \\ &\quad - {}^{r}\boldsymbol{\omega}^{\top}[{}^{r}\boldsymbol{y}_{sen}]_{\times}\boldsymbol{K}\Delta\,{}^{r}\boldsymbol{y}_{sen} \\ &= -\boldsymbol{v}^{\top}\boldsymbol{b}_1 - \boldsymbol{\omega}^{\top}\boldsymbol{b}_2 - \gamma\,\|{}^{r}\boldsymbol{\omega}\|^2 \le 0, \end{aligned} \tag{59}$$

where γ is positive scalar. The closed-loop dynamics (57) was used in the derivation. The time derivative is semi-negative de nite and the system is stable. From the LaSalle's invariant theorem [22], the state of the system that remains in a neighborhood of the desired point asymptotically approaches the set de ned by

$${}^{w}\boldsymbol{R}_r\left\{\boldsymbol{h}_g - \boldsymbol{P}_{s_{v_1}}^{\top}\boldsymbol{K}_v\Delta\boldsymbol{s}_v\right\} = \mathbf{0}, \tag{60}$$

$$\boldsymbol{G}^{\top}\left\{\boldsymbol{H}_h^{\top}\Delta\boldsymbol{s}_h + \boldsymbol{P}_{s_{v_2}}^{\top}\boldsymbol{K}_v\Delta\boldsymbol{s}_v + [{}^{r}\boldsymbol{y}_{sen}]_{\times}\boldsymbol{K}\Delta\,{}^{r}\boldsymbol{y}_{sen}\right\} = \mathbf{0}. \tag{61}$$

${}^{w}\boldsymbol{R}_r$ is non-singular, therefore, the vector in the parenthesis of Equation (60) must be zeros. From (43) and (44), the vector in the parenthesis of Equation (60) is given as

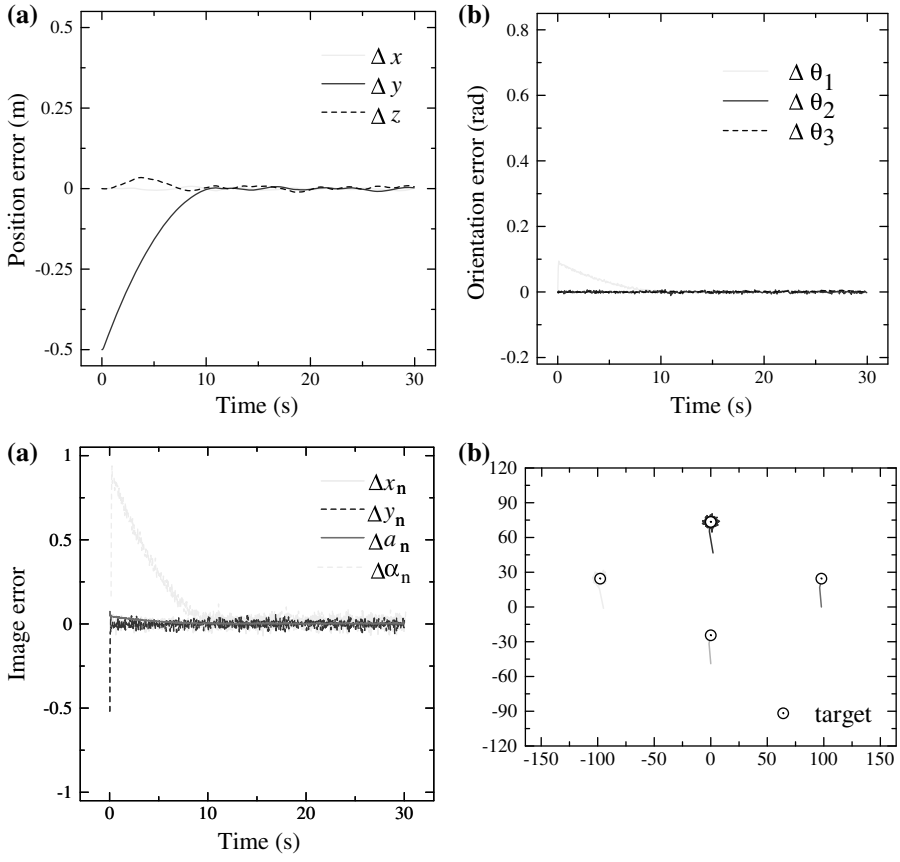

Figure 13. Simulation results in Case 7, con gured as Figure 7.

Downloaded by [Inria Rocquencourt] at 08:14 05 April 2013

x_n, y_n, and α converge to zero because $\mathcal{T}$ is non-singular. Thus, we proved that the equilibrium point of the UAV is asymptotic stable.

6. Simulation

In this section, six selected simulations are presented to validate the effectiveness of the proposed controller using the conditions given in Table 1, and these gains were tuned through some preliminary simulations. The UAV has four propellers and its transmission matrix A is given as follows:

$$\boldsymbol{A} = \begin{bmatrix} 0 & 0 & 1 & 0 & -\ell & \kappa \\ 0 & 0 & 1 & \ell & 0 & -\kappa \\ 0 & 0 & 1 & 0 & \ell & \kappa \\ 0 & 0 & 1 & -\ell & 0 & -\kappa \end{bmatrix}, \qquad (65)$$

where ℓ is the length of the moment arm, and κ is a ratio between the translational force to the rotational torque. The following parameters are used for the simulations: $m = 0.90\,(\mathrm{kg})$, $\ell = 0.30\,(\mathrm{m})$, $I = (1.20, 1.20, 2.00) \times 10^{-3}\,(\mathrm{kgm}^2)$, and $\kappa = 0.0158\,(\mathrm{m})$. The damping terms are modeled as the quadratic form of the velocities arising from the aerodynamics [20] and de ned as follows:

$$\boldsymbol{b}_1 = d_1 \boldsymbol{Q}({}^{s}\boldsymbol{v})\,{}^{s}\boldsymbol{v}, \quad \boldsymbol{b}_2 = d_2 \boldsymbol{Q}({}^{s}\boldsymbol{v})\,{}^{s}\boldsymbol{v}, \qquad (66)$$

where $\boldsymbol{Q}(\boldsymbol{a})$ is a diagonal matrix and the ith diagonal element is absolute value of the ith element of $\boldsymbol{a}$. The damping coef cients d_1 and d_2 are modeled as constant, based on experimental results in [23], and given in Table 2. The visual data is updated every 33 ms except Case 4, while ${}^{s}\boldsymbol{v}$, ${}^{s}\boldsymbol{\omega}$, and $\boldsymbol{\theta}$ are measured and the control input is updated every 1 ms. We use four feature points, which are distributed around the origin of the base frame. As shown in Table 2, in Cases 1 to 4, the initial con guration is assigned so that the UAV goes from the vicinity to the above of the base frame. In Case 5, the initial con guration is assigned so that the UAV goes away from the above of the base frame. The differences in each con guration are shown in the image sampling time, the feedback gain, γ. In Case 6, a Gaussian noise with mean zero and standard deviation 2 pixels, which correspond to about 7.5 (mm) in the horizontal plane, 0.5 (m) above on the target, is added to the image. Other conditions are the same in Case 1. In Case 7, the UAV goes to the target on the same horizontal plane to validate the pure translational motions attained by the virtual spring approach. Other conditions are the same in Case 6.

Figures 7–11 show the translation and orientation errors of each case as well as the image features error and the image points trajectory. In Case 1, a good damping is used as shown

in Table 2, and the errors converge to zero around 15 s. In Case 2, less damping in the translational directions is used as shown in Table 2. Then, the system is under-damped and the convergence is retarded compared to Case 1. In Case 3, the damping feedback in the rotational directions is not used. Then, residual errors remain and the motion becomes vibrationally as in a limit cycle. This is due to the sampling time of the visual data. This motion is improved using 10-ms image sampling time as shown in Case 4, where the less damping in the translational directions and no damping feedback in the rotational directions are used, as well as using larger rotational damping as shown in Case 2.

In Case 5, the convergence is a little bit slower than in Case 1 because of the difference of the desired con guration. We can get the better performance when the landmarks are just below the UAV at a desired con guration. Indeed, the interaction matrix plays role of the moment arm of the image error, and the desired con guration in Case 5 becomes more sensitive to the image error than in Cases 1 to 4.

In Case 6, image errors appeared due to the introduction of the image noise. These errors induced some vibrations in the position and orientation of the UAV. However, the controller attenuated the vibrations and the magnitudes are smaller than those in the image. The proposed scheme is thus robust with respect to image noise.

In Case 7, the UAV approached to the target as the exponential maps and the image errors are almost straight lines.

7. Conclusion

This paper proposed an IBVS for controlling the position and the orientation of a UAV with a xed camera, which points the downward direction. The transpose Jacobian control from image moments is used to control the translational and the rotational motions in the vertical axis. On the other hand, the lateral motion cannot be generated with this method due to the under-actuation of UAVs. Positive feedback structure of the image errors to the lateral motion was revealed, and a virtual spring was introduced to stabilize the pose of the UAV. Simulations showed that this method is effective to control the pose of a UAV, even if the low sampling rate of the visual data and the image errors may cause some residual errors. We also showed that it is better to put the landmarks right below the desired pose of the UAV.

Future works will be devoted to realize experiments on a real platform. The current controller depends on the perspective image moment, and the controller is also undergoing to be generalized to algorithms, which can use any other image features, and camera con guration.

Acknowledgements

We would like to thank Professor Tarek Hamel from I3S-CNRS, Nice-Sophia Antipolis, for his valuable comments and Dr. Nicolas Guenard from CEA/LIST for his valuable information of the parameters used in the simulation.

Notes on contributors

Ryuta Ozawa received his B.S. degree in precision engineering and M.S. and Ph.D. degrees in mechanical engineering from Meiji University, Kanagawa, Japan, in 1996, 1998, and 2001, respectively. From 1999 to 2002, he was a research assistant with Meiji University. In 2002, he was a research fellow with the Japan Society for the Promotion of Science. He is currently an associate professor with Ritsumeikan University, Kusatsu, Japan. His current research interests include tendon-driven mechanisms, elastic joint robots, visual servoing, and control of robotic hands and bipeds.

François Chaumette was graduated from École Nationale Supérieure de Mécanique, Nantes, France, in 1987. He received his Ph.D. degree in computer science from the University of Rennes, France, in 1990. Since 1990, he has been with Inria in Rennes where he is now "Directeur de Recherches" and head of the Lagadic group (http://www.irisa.fr/lagadic). His research interests include robotics and computer vision, especially visual servoing and active perception. Chaumette received the AFCET/CNRS Prize for the best French thesis in automatic control in 1991. He also received with Ezio Malis the 2002 King-Sun Fu Memorial Best IEEE Transactions on Robotics and Automation Paper Award. He has been associate editor of the IEEE Transactions on Robotics from 2001 to 2005 and is now in the Editorial Board of the International Journal of Robotics Research.

References

[1] DeGarmo MT. Issues concerning integration of unmanned aerial vehicles in civil airspace. Technical report, MITRE, Center for Advanced Aviation System Development, McLean, Virginia, 2004.

[2] Tayebi A, McGilvray S. Attitude stabilization of a VTOL quadrotor aircraft. IEEE Trans. Control Syst. Technol. 2006;14:562–571.

[3] Hamel T, Mahony R, Lozano R, Ostrowski J. Dynamic modelling and con guration stabilization for an X4- yer. Barcelona: In IFAC World Congress; 2002.

[4] Thrun S, Burgard WD, Fox D. Probabilistic robotics. Cambridge: MIT press; 2006.

[5] Chaumette F, Hutchinson S. Visual servo control part I: basic approaches. IEEE Robot. Automat. Mag. 2006;18:82–90.

[6] Altug E, Ostrowski JP, Mahony R. Control of a quadrotor helicopter using visual feedback. In: Proceedings of IEEE International Conference on Robotics and Automation; 2002 May; Washington, DC. p. 72–77.

[7] Watanabe K, Yoshihata Y, Iwatani Y, Hashimoto K. Image-based visual PID control of a micro helicopter using a stationary camera. Adv. Robot. 2008;22:381–393.

[8] Michael N, Mellinger D, Linsdsey Q, Kumar V. The GRASP multiple micro-UAV test bed. IEEE Robot. Autom. Mag. 2010;17:56–65.

[9] Azrad S, Kendoul F, Nonami K. Visual servoing of quadrotor micro-air vehicle using color-based tracking algorithm. J. Syst. Des. Dyn. 2010;4:255–268.

Downloaded by [Inria Rocquencourt] at 08:14 05 April 2013

[10] Hamel T, Mahony R. Visual servoing of an under-actuated dynamic rigid-body system: an image-based approach. IEEE Trans. Robot. Autom. 2002;18:187–198.
[11] Hamel T, Mahony R. Image based visual servo control for a class of aerial robotic systems. Automatica. 2007;43:1975–1983.
[12] Guenard N, Hamel T, Mahony R. A practical visual servo control for an unmanned aerial vehicle. IEEE Trans. Robot. 2008;24:331–340.
[13] Mahony R, Corke P, Hamel T. Dynamic image-based visual servo control usig centroid and optic ow features. ASME J. Dyn. Syst. Meas. Contr, 2008;130:011005.1–011005.12.
[14] Bras FL, Mahony R, Hamel T, Binetti P. Dynamic image-based visual servo control for an aerial robot: theory and experiments. Int. J. Optomechatronics. 2008;2:296–325.
[15] Bourquardez O, Mahony R, Guenard N, Chaumette F, Hamel T, Eck L. Image-based visual servo control of the translation kinematics of a quadrotor aerial vehicle. IEEE Trans. Robot. 2009;25.
[16] Tahri O, Chaumette F. Point-based and region-based image moments for visual servoing of planar objects. IEEE Trans. Robot. 2005;21:1116–1127.
[17] Takegaki M, Arimoto S. A new feedback method for dynamic control of manipulators. ASME J. Dyn. Syst. Meas. Contr. 1981;102:119–125.
[18] Ozawa R, Chaumette F. Dynamic visual servoing with image moments for a quadrotor using a virtual spring approach. In: Proceedings - IEEE International Conference on Robotics and Automation; 2011 May; Shanghai, China. p. 5670–5676.
[19] Yun X, Bachmann ER, McGhee RB. A simpli ed quaternion-based algorithm for orientation estimation from earthgravity and magnetic eld measurements. IEEE. Trans. Instrum. Meas. 2008;57:638–650.
[20] Mahony R, Kumar J, Corke P. Multirotor aerial vehicles. IEEE Robot. Autom. Mag. 2012;19:20–32.
[21] Goldstein H, Poole CP, Safko JL. Classical mechanics. 3rd ed. Pearson Education; 2001.
[22] Arimoto S. Control theory of non-linear mechanical systems: a passivity-based and circuit-theoretic approach. Oxford Science Publications. Oxford University Press;1996.
[23] Derafa L, Madani T, Benallegue A. Dynamic modeling and experimental identi cation of four rotors helicopter parameters. In: Proceedings of the IEEE International Conference on Industrial Technology; 2006 Dec. p. 1834–1839.